Dry Fuel Jet Half-Angle Measurements and Correlation for an Entrained Flow Gasifier

Authors:

Francis Kus, Robin Hughes, Arturo Macchi, Poupak Mehrani, Marc Duchesne

Abstract:

Reduced order models (ROMs) are increasingly applied to entrained flow gasification development due to reduced computational requirements relative to computational fluid dynamics (CFD) models. However, they require greater a posteriori knowledge of the reactor physics. A significant parameter influencing ROM outputs is the jet half-angle of the solid fuel and oxidant mixture in the gasifier. Thus, it is important to understand the geometry of the jet in the gasifier, and how it is dependent on operating parameters, such as solid and carrier gas flow rates. In this work, an existing model for jet half-angles, which considers the ratio of surrounding gas density to jet core density, is extended to a dry solids jet with impinging gas. The model is fitted to experimental jet half-angles. The jet half-angle of a non-reactive flow was measured using laser-sheet imaging for solid fluxes in the range of 460?880 kg/m²·s and carrier gas fluxes in the range of 43?90 kg/m²·s at the transport line outlet. Jet half-angles ranged from 5.6° to 11.3°, increasing with lower solid/gas loading ratios. CFD simulations of two reactive conditions, with solid and gas fluxes similar to experiments, were used to test the applicability of the proposed jet half-angle model.

Dry Fuel Jet Half-Angle Measurements and Correlation for an Entrained Flow Gasifier [†]

Francis Kus [1], Robin Hughes [2], Arturo Macchi [1], Poupak Mehrani [1] and Marc Duchesne [2],*

[1] Department of Chemical and Biological Engineering, University of Ottawa, Ottawa, ON K1N 6N5, Canada; francistkus@gmail.com (F.K.); arturo.macchi@uottawa.ca (A.M.); poupak.mehrani@uottawa.ca (P.M.)

[2] Natural Resources Canada, CanmetENERGY-Ottawa, Ottawa, ON K1A 1M1, Canada; robin.hughes@canada.ca

* Correspondence: marc.duchesne@canada.ca; Tel.: +1-613-947-0287

Abstract: Reduced order models (ROMs) are increasingly applied to entrained flow gasification development due to reduced computational requirements relative to computational fluid dynamics (CFD) models. However, they require greater a posteriori knowledge of the reactor physics. A significant parameter influencing ROM outputs is the jet half-angle of the solid fuel and oxidant mixture in the gasifier. Thus, it is important to understand the geometry of the jet in the gasifier, and how it is dependent on operating parameters, such as solid and carrier gas flow rates. In this work, an existing model for jet half-angles, which considers the ratio of surrounding gas density to jet core density, is extended to a dry solids jet with impinging gas. The model is fitted to experimental jet half-angles. The jet half-angle of a non-reactive flow was measured using laser-sheet imaging for solid fluxes in the range of 460–880 kg/m^2·s and carrier gas fluxes in the range of 43–90 kg/m^2·s at the transport line outlet. Jet half-angles ranged from 5.6° to 11.3°, increasing with lower solid/gas loading ratios. CFD simulations of two reactive conditions, with solid and gas fluxes similar to experiments, were used to test the applicability of the proposed jet half-angle model.

1. Introduction

Greenhouse gas emissions over the past 100 years have greatly increased, resulting in an increased demand for clean alternative processes [1]. Integrated gasification combined cycle (IGCC) power plants are considered one of the more attractive technologies for clean power production, due to higher efficiency when compared to conventional power production with carbon capture, and easier gas cleaning due to higher component concentrations in the product gas [2]. The IGCC process includes a gasification unit that converts carbonaceous fuel to a gaseous mixture of CO and H_2 known as synthesis gas, or "syngas". The syngas can be easily treated and/or purified for further use.

A better understanding of the impact of operational changes during the gasification process has been a research topic for many years. Computational fluid dynamics (CFD) is often used to increase understanding in the field due to the high operational costs associated with experimental trials [3,4]. Advantages of CFD models include detailed multi-phase sub-models that can provide insight into the hydrodynamics and kinetics of the reactions. A major drawback of CFD modelling is the computation time; a CFD simulation for one condition can take several days with high computational power.

Reduced order models (ROM) are an alternative to CFD modelling. They require less computational time and power; simulation typically requires several minutes on a standard work station. The reduced computational time is amenable to studying detailed reaction kinetics and the transient performance of gasifiers [5–7]. ROMs function on a basis of a reactor network that emulates the geometry and fluid dynamics of the gasifier. As a result of not simulating the complete multi-phase dynamics of the system, to accurately represent the gasifier, a ROM requires a posteriori knowledge of the geometry of the solid flow inside the reactor, of which the solid jet half-angle has a significant impact.

Sahraei et al. proposed a ROM for an entrained flow gasification unit located at CanmetENERGY in Ottawa, Canada [5,6,8,9]. Their reactor network model consists of three plug-flow reactors (PFR) and two continuous-stirred tank reactors (CSTR). The three PFRs represent jet expansion zones and one down-stream zone, while the CSTRs represent recirculation zones in the reactor (Figure 1). The geometry of the reactor models are influenced by the solid jet half-angle in the reactor vessel, which has been shown to have a significant effect on the carbon conversion and composition of the syngas produced [8,10].
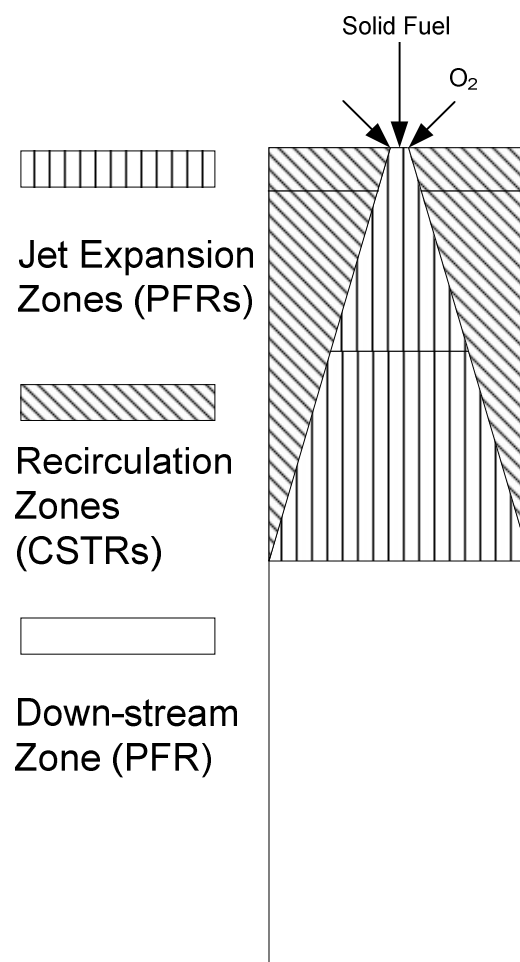
Figure 1. Reactor network model representing the different reactor zones within the entrained flow gasification unit at CanmetENERGY.

Lack of experimental data in the area of solid jet geometry for gasification systems has resulted in ROMs acquiring jet geometries from CFD simulations or from published values from swirl jets in combustion systems [5,10]. Consequently, it is of interest to model how the solid jet half-angle in entrained flow gasifiers varies with changing operating conditions such as the solid flux and the

solid/gas loading ratio (m^*). The solid/gas loading ratio is defined as the ratio of mass flow rate of solids (m_s) to the mass flow rate of gas (m_g):

$$m^* = m_s/m_g \tag{1}$$

Thus, in this work, an existing model for jet half-angles is extended to multiphase conditions relevant to gasification of a dry solid fuel co-injected with impinging gas. Experimental data of jet half-angles for a downdraft-entrained flow gasifier with non-reactive conditions at relatively high solid/gas loading ratios are obtained via digital laser sheet imaging and pixel analysis, analyzed for variability, and fitted to the jet half-angle model. The model is then applied to reactive operating conditions with predictions compared to jet half-angles estimated via CFD simulations.

2. Theory

2.1. Previous Studies

In the past, studies of two-phase jets have focused largely on the influence of the dispersed phase on the velocity profiles and stability of the jet. Hedman and Smoot determined velocity profiles for two-phase jets of aluminum powder in helium and air [11]. Modarress determined that solids reduce gas velocity fluctuations [12]. Fleckhaus et al. studied the stability and flow structure of a solid-laden jet, and found that the spreading rate of a two-phase jet is smaller than that of a single-phase jet [13]. Numerical studies have also been performed on solid-laden jets with good agreement with available experimental data [14–16]. However, it should be noted that most work regarding solid-laden jets has been done with a relatively low solid loading ratio of $m^* < 1$. Limited studies performed on dense jets have found that increasing the solid loading ratio beyond the range of $m^* \approx 1$ further reduces velocity fluctuations and the spreading rate [17].

It is of interest to determine the half-angle of a gas-solid jet, and determine how it varies with operating parameters such as solid flow and gas flow injected into the reactor. While modelling of jet half-angles for solid-laden jets is limited, Liu et al. found that dense gas-solid jets behave similarly to liquid jets, implying the jet of dispersed particles flow like a pseudo-homogeneous fluid [18].

Jet half-angles have been studied in depth for single-phase liquid and gas systems. Ranz, and later Reitz and Bracco discussed the momentum balance in a liquid jet and outlined important parameters defining spray dispersion; the square root of liquid jet density and liquid jet velocity [19,20]. Wu et al. studied the jet half-angle of liquid-atomizing jets and found that the influence of the aforementioned parameters holds at high pressures [21]. Roy et al. studied subcritical and supercritical fluoroketone jets, and found that the jet half-angle is proportional to the square root of the ratio of the density of the jet surroundings, ρ_a, to the density of the jet core at the injection point, ρ_0, for both subcritical and supercritical jets [22]. They proposed a simple model for the jet half-angle (φ), where a is a constant that is dependent on system geometry and fluid properties:

$$\varphi = a\left(\frac{\rho_a}{\rho_0}\right)^{0.5} \tag{2}$$

2.2. Model Extension

The model presented by Roy et al. (Equation (2)) can be extended to conditions pertinent to entrained flow gasification of a dry fuel. An underlying physical difference between reactive and non-reactive systems is the surrounding gas temperature. While non-reactive flows will maintain an ambient temperature (approximately 300 K) throughout the system, reactive conditions can have temperatures in excess of 2000 K for gas surrounding the jet. The surrounding gas density is inversely proportional to the temperature, following the ideal gas law. Thus, the jet half-angle for reactive systems is expected to be lower than the half-angle for non-reactive systems. Beér and Chigier have reported a similar observation [23]. For a solid suspension jet, the density of the jet, ρ_0, is a function of

the jet's solid/gas loading ratio, gas density, and solids density. If the solids density is much greater than the gas density, then the density of the jet can be expressed as a function of the jet's solid/gas loading ratio, and gas density:

$$\rho_0 = \left(\frac{m^* + 1}{1 + m^* \rho_g / \rho_s} \right) \rho_g \approx (m^* + 1) \rho_g \tag{3}$$

Thus, increasing the solid/gas loading ratio will reduce the jet half-angle. Note that gas impinging into the jet, at the point of solid injection, must be accounted for in the mass of gas used to calculate the solid/gas loading ratio (Equation (1)), and in the gas density used in Equation (3). However, this will only apply for gas impingement that is nearly parallel to the jet flow, and may not apply to gas impingement that is nearly perpendicular to jet flow.

3. Experimental Setup

A pressurized gasification pilot plant, discussed in previous work [24], was used to conduct a jet geometry analysis on a high pressure non-reactive pneumatic conveying system, using the solid injector design shown in Figure 2. The solid injector consists of a center tube (internal diameter = 6.2 mm) that conveys a mixture of solids and carrier gas into the reactor, and a series of eight impinging jets (ID = 2.5 mm), injecting gas at an angle of 37°, to mix an impinging gas into the solid-gas jet. Additionally, an outer concentric annulus introduce sleeve gas into the reactor. For reactive conditions, the impinging gas is O_2, while the sleeve gas is steam. For non-reactive conditions, nitrogen is used as carrier, impinging and sleeve gas. The pulverized solid used in the study is petroleum coke (particle harmonic mean size from a mass distribution of 10 μm, density of 1176 kg/m^3) [24].
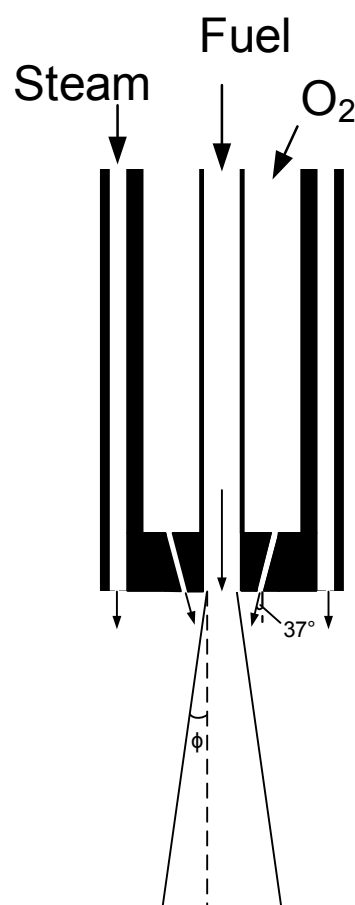

Figure 2. Downdraft entrained flow gasifier solids injector.

The jet geometry imaging was done using a Phantom v9.1 camera (Vision Research, Wayne, NJ, United States), with an image capture frequency of 10 Hz and a resolution of 1632 × 1200 pixels, and a Nano L Nd:YAG laser (Litron Lasers, Warwickshire, England) producing a laser sheet with a thickness of 5 mm on which the images were captured. The laser sheet was in line with the centre of the jet injected by the solids injector. It should be noted that an analysis was done to study the importance of centering the laser, and found that an offset of as little as 7 mm resulted in skewed jet angles recorded by the imaging software. The camera and laser setup is depicted in Figure 3, and discussed in more detail by Daviault et al. [25]. The imaging process was done over a period of 30 s for each test, generating 300 images per test.
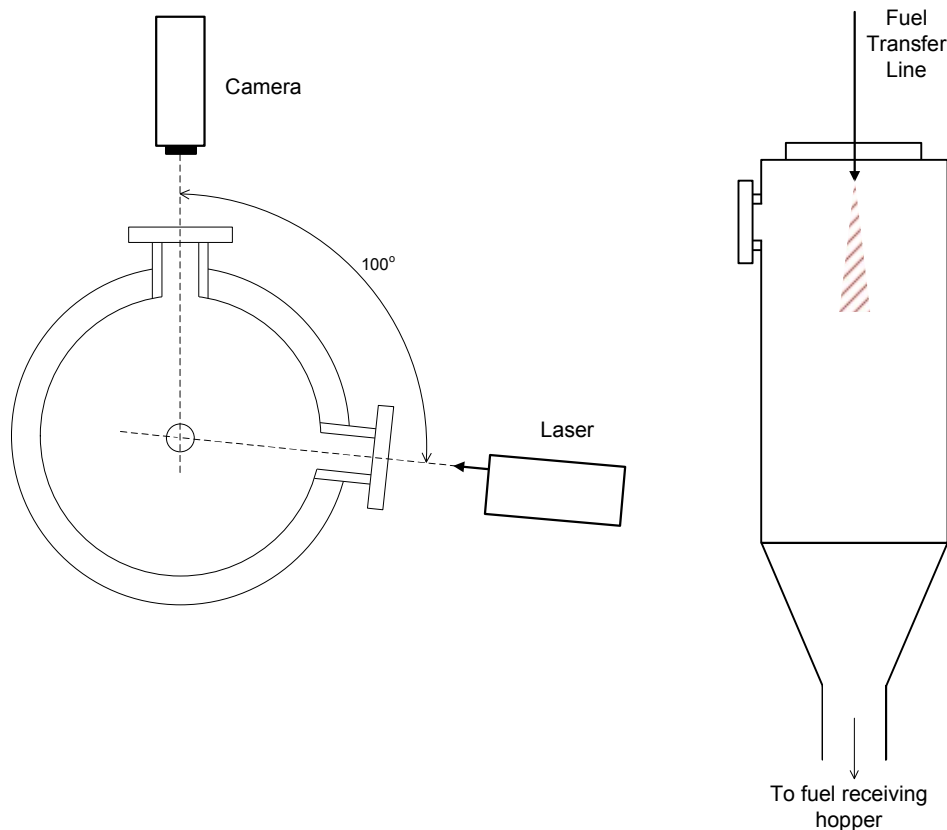

Figure 3. Schematic of the pneumatic transport system's visualization spool; cross-sectional top view (**left**) and side view (**right**).

A mean image was generated from the 300 images taken for each test using DynamicStudio software (version 3.41, Dantec Dynamics, Skovlunde, Denmark), and the mean jet angle was measured using the software's built-in spray characterization tool, which measures jet angle using a pixel detection method. The software measures pixel color contrasts to determine the edge of the spray, and measures the jet angle based on this criterion (see Figure 4). The jet boundary is thus defined by the software as the point at which the particle density is too low to provide an image contrast with the laser sheet. The measurements were taken over an axial distance from the solids injector orifice to a distance of 84 mm downstream of the solids injection.

Three tests were performed at each condition to determine the mean jet angle. The error reported in the tables herein represent the standard deviation of the jet angle found for the three tests at each condition. Image masking ensured that the software did not account for recirculating particles as individual jets. Due to the density of solids in the jet, the laser sheet was unable to penetrate completely through the jet. Thus, only one side of the jet was illuminated resulting in a single side of the jet being captured in the images. The jet was assumed to be axisymmetrical. Most tests were performed at room

temperature and a pressure of 1600 kPa (measured inside the receiving vessel in which the solids are injected), with a series of tests performed at room temperature and a pressure of 800 kPa. An inert gas was used as the carrier, impinging and sleeve gas to prevent ignition due to electrostatic discharge while conveying; this is in addition to the grounding of the system. It should be noted that electrostatic charge could potentially influence the jet half-angle generated as the conveying stream is injected into the receiving vessel. Nitrogen was selected for impinging gas due to its low cost and similar physical properties to oxygen (similar gas densities and viscosities). Nitrogen was also used in place of steam for the sleeve gas, in order to preserve the dry state of the solids, and to allow recycling of the solids in the conveying system.
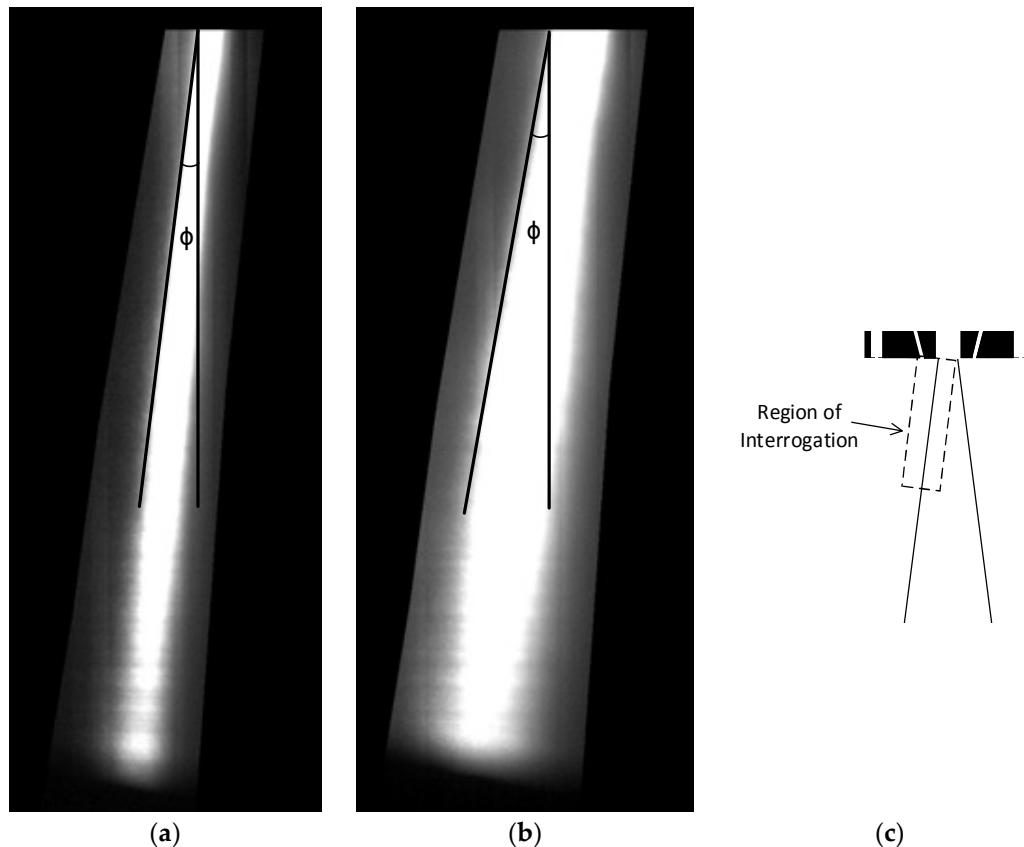
Figure 4. Resulting image mean generated from a set of data encompassing 300 images taken at a frequency of 10 Hz. (**a**): solid/gas loading ratio 7.3 kg_{solid}/kg_{gas}, without impinging gas; (**b**): solid/gas loading ratio 7.2 kg_{solid}/kg_{gas}, with impinging gas; (**c**): schematic indicating the region of interrogation.

The conditions analyzed were chosen to complement work done on the pneumatic conveying of the pulverized solids [24], as well as to emulate hot flow conditions of CanmetENERGY's pilot-scale gasifier [26]. Solid flux was in the range of 460–880 $kg/m^2 \cdot s$, with gas flux in the range of 43–90 $kg/m^2 \cdot s$. Jet geometries were analyzed with and without the influence of sleeve and impinging gas.

4. Results and Discussion

4.1. Experimental Results

Gas impingement was initially omitted to observe the influence of flow conditions on the jet angle without external interaction. The solid/gas loading ratio (m^*) in the conveying line was observed to have a direct impact on the jet half-angle; as the loading ratio is increased, the jet half-angle decreases

(Table 1). In order to ensure this is not a direct result of varying individual flow rates, two test conditions with similar loading ratios ($\pm 1\%$) are compared. Conditions 3 and 4 result in the same jet half-angle despite a difference in solid flow of 12% and a difference in gas flow of 11% (Table 1). For the cases with gas impingement, the impinging gas flow rate was approximately four times larger than the conveying gas flow rate (40 kg/h compared to 8–10 kg/h). As shown in Table 1, the relation between the loading ratio and jet half-angle holds true when introducing impinging gas; all cases with impinging gas have a lower loading ratio and thus a higher jet half-angle than all cases without impinging gas. For the cases with impinging gas (i.e., conditions 10–13), the changes in loading ratio were not sufficient to have a significant impact on the jet half-angle. The sleeve gas flow rate was also varied between two values of 0 and 10 kg/h N_2. These values were selected based on hot flow conditions used with CanmetENERGY's pilot-scale gasifier, which was operated with a steam (i.e., sleeve gas) flow rate of up to 20 kg/h H_2O [26]. A value of 10 kg/h N_2 was selected to remain within the range of momentum of the steam entering the reactor (10 kg/h N_2 having the momentum equivalent of 8 kg/h H_2O). The flow of sleeve gas did not impact the jet half-angle during cold flow testing (e.g., condition 11 vs. condition 13 in Table 1). However, during reactive conditions the introduction of steam as sleeve gas may influence the jet half-angle by affecting the temperature surrounding the jet, which should influence the jet half-angle as discussed in the Theory section.

Table 1. Influence of solid and gas flow rates on jet half-angle.

Condition Number	Solid Flow (kg/h)	N_2 Gas Flows (kg/h)			Pressure (kPa)	Loading Ratio (kg_{solid}/kg_{gas})	Jet Half-Angle (°)
		Conveying	Impinging	Sleeve			
1	81	4.7	0	0	1600	17.34	5.6 ± 0.1
2	95	6.2	0	0	1600	15.26	5.9 ± 0.2
3	84	5.7	0	0	1600	14.75	6.1 ± 0.1
4	74	5.1	0	0	1600	14.61	6.0 ± 0.1
5	62	7.8	0	0	1600	7.98	6.4 ± 0.2
6	71	9.7	0	0	1600	7.32	6.4 ± 0.2
7	54	7.9	0	0	1600	6.85	6.7 ± 0.2
8	27	7.4	0	10	800	3.65	8.9 ± 0.2
9	25	7.5	0	0	800	3.33	10.0 ± 0.2
10	69	9.6	40	10	1600	1.39	11.3 ± 0.2
11	53	8.7	40	0	1600	1.09	11.3 ± 0.1
12	52	9.4	40	10	1600	1.05	11.3 ± 0.1
13	50	8.7	40	10	1600	1.03	11.1 ± 0.1

4.2. Jet Half-Angle Variability

It is important to track jet half-angle variability as it affects gasifier operation, and can potentially lead to unsafe conditions and/or poor syngas quality. The jet half-angle standard deviation was determined using 300 images taken for select conditions in order to determine the influence of the solid/gas loading ratio, impinging gas flow, and sleeve gas flow. Table 2 shows the jet half-angle mean value and standard deviation for each test, as well as the corresponding conditions for each test (loading ratios and various gas flows). Note that the jet half-angles in this table vary slightly from those in Table 1 since they were determined by measuring angles for each image in a set of 300 images. In contrast, values in Table 1 are from measuring the angles from 3 images which are each the result of averaging 300 images. An F-test, with a 90% confidence interval, was applied to determine the significance of the different standard deviations measured for each condition. The results indicate that conditions 4 and 6 have statistically similar variance, as well as conditions 10, 11 and 13. The analysis thus suggests that the presence of the impinging gas influences the variability of the jet half-angle. The presence of the sleeve gas, as well as varying the solid/gas loading ratio (excluding the impinged gas), was found to not influence the variability of the jet half-angle. For certain applications, it may be more important to minimize the relative variability, represented by the coefficient of variation, rather than the (absolute) variability, represented by the standard deviation. The coefficients of variation,

i.e., the ratios of the standard deviation to the mean, are included in Table 2 and are similar for all conditions.

Table 2. Comparison of standard deviations of jet half-angles for different operating conditions.

Condition Number	4	6	10	11	13
solid/gas loading ratio [a]	14.6	7.3	7.2	6.1	5.7
solid/gas loading ratio [b]	14.6	7.3	1.4	1.1	1.0
impinging gas (kg/h)	0	0	40	40	40
sleeve gas (kg/h)	0	0	10	0	10
mean jet half-angle (°)	5.9	6.2	9.4	10.2	9.8
half-angle standard deviation (°)	0.6	0.6	1.0	1.1	1.1
half-angle coefficient of variation	0.10	0.10	0.11	0.11	0.11

[a] excluding impinged gas in the calculation; [b] including impinged gas in the calculation.

Beyond the magnitude, whether absolute or relative, of the jet half-angle variability, the frequency of the variability can also have an impact on gasifier performance. For instance, reactor temperatures and syngas composition are sensitive to the jet angle [8]; hence, changing the frequency of the jet half-angle variability could cause refractory thermal shock or syngas consistency issues. Furthermore, analyzing the variability in the frequency domain can help determine causes of the variability. The data for the conditions presented in Table 2 were subjected to a fast Fourier transformation to analyse the data in the frequency domain. Frequency spectra are shown in Figure 5. Conditions 4 and 6 have similar frequency spectra; they do not have a mean squared amplitude greater than $0.01°^2$ at frequencies greater than 0.3 Hz. Conditions 10, 11 and 13 have similar frequency spectra; they have several frequencies with amplitudes of $0.01–0.03°^2$ in the range of 0.3–5.0 Hz. The added variability with impinging gas, i.e., conditions 11, 10, and 13, could be a result of high frequency, i.e., >0.3 Hz, fluctuations in the control valve position for the impinging gas; the control valve (Samson Type 3760 Electropneumatic Positioner, Samson Controls Inc., Markham, ON, Canada) requires ≤2 s to transit from fully open to fully closed. This highlights how operating conditions can be sensitive to certain aspects of control systems.

(a)

Figure 5. *Cont.*

(b)
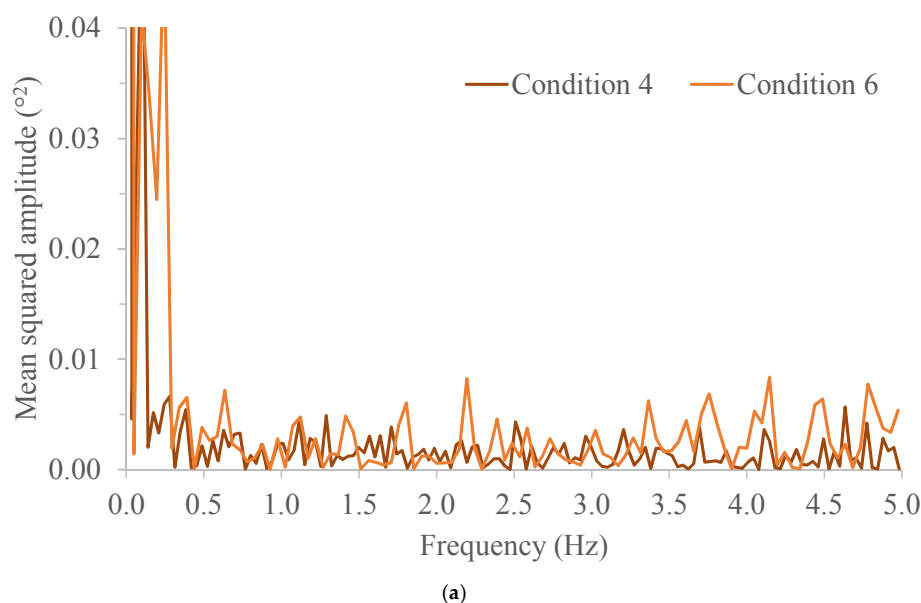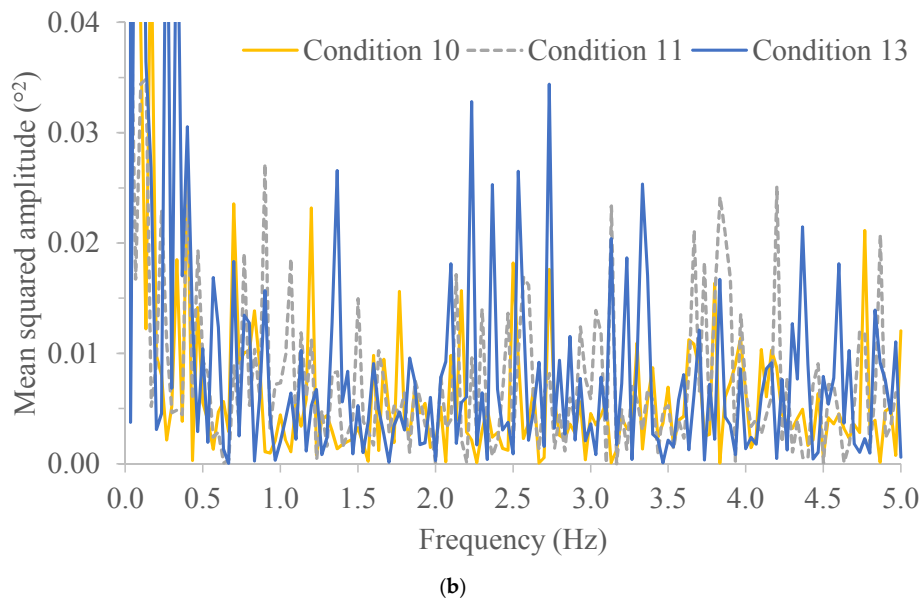
Figure 5. Frequency analysis. Details of conditions are reported in Table 2. (**a**) Conditions 4 and 6; (**b**) Conditions 10, 11 and 13.

4.3. Model Fitting

The relationship put forth by Roy et al. (Equation (2)) shows that the jet half-angle is inversely proportional to the jet core density. This dependence is extended to the solid/gas loading ratio, m^*, via Equation (3); as the solid/gas loading ratio increases, the density of the suspension also increases. Thus, the jet half-angle should be inversely proportional to the solid/gas loading ratio. This relationship is exemplified in Table 1, where the jet half-angle increases as the solid/gas loading ratio decreases.

Least squares regression was applied to the experimental data (i.e., conditions 1–13 in Table 2) with Equation (2) and yielded a value of 17.3 for constant *a*. The coefficient of determination, average absolute relative error and bias factor (as presented by Macchi et al. [27]) of the resulting model are 0.86, 10% and 0.93, respectively. The model is compared to experimental results in Figure 6. The application of a model including the square-root of density ratios implies that the jet half-angle can be related to the entrainment of surrounding gas into the jet, for the system and operating conditions at hand (solid/gas loading ratios varying from 1–18 kg_{solid}/kg_{gas}; solid fuel flow rates ranging from 25–100 kg/h; conveying gas flow rates ranging from 4.7–10 kg/h, and impinging gas flow rates up to 40 kg/h). Note that these conditions correspond to density ratios ranging 0.07–0.5.
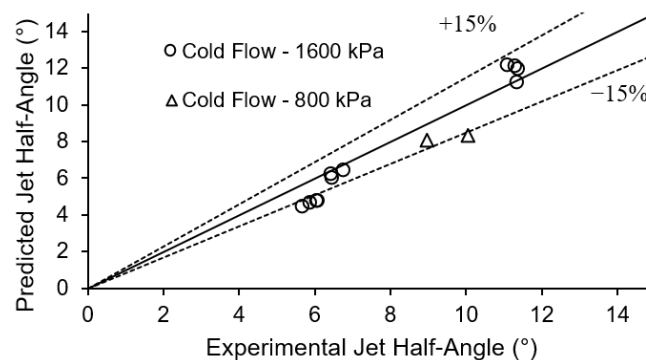

Figure 6. Comparison of jet half-angle predictions and experimental values.

Two CFD simulations, with similar conditions as the experiments [28], were analyzed to determine the jet half-angle for reactive flow (Table 3). The jet core in both cases remains at ambient temperature (~300 K), while the surrounding temperatures differ between the two cases; estimated at 1231 K and 1165 K for cases 1 and 2, respectively (Figure 7). The jet half-angles, estimated using particle volume fraction thresholds, are, respectively, 3.6–5.2° and 4.6–6.7° (Figure 8). The particle volume fraction thresholds, i.e., 2.5×10^{-4}–1.0×10^{-3}, were selected based on the range of the solids volume fraction in the bulk jet surroundings. Similarly, change in mean particle volume fraction is used to define the characteristics lengths of gas jets penetrating into a fluidized bed [29]. Also indicated in Table 3 are the jet half-angles predicted using the same correlation that was applied to the cold flow cases, i.e., Equation (2) with an *a* factor of 17.3, which falls within the predicted value boundaries of the CFD simulations. However, although the CFD results suggest that the impact of increased surrounding temperature is greater than the increased loading ratio, leading to a rise in jet half-angle from case 1 to 2, the proposed model predicts a negligible difference in jet half-angles. Since the injector geometries are the same for the experiments and CFD simulations, further investigation is required to determine whether the difference in CFD and proposed model predictions are due to the proposed model not explicitly accounting for gradients in the surrounding temperature and the solids volume fraction.

Table 3. Properties of the computational fluid dynamics (CFD) simulation cases.

Case	Solid Flow (kg/h)	Gas Flows (kg/h)			Loading Ratio	Surrounding Temperature (K)	CFD Half-Angle [a] (°)	Equation (2) Half-Angle (°)
		Carrier N_2	Impinging O_2	Sleeve H_2O				
1	41	8.2	37.2	10.7	0.90	1231	3.6–5.2	5.1
2	60	7.5	43.6	10.2	1.17	1165	4.6–6.7	4.9

[a] estimated using solids volume fraction thresholds of 2.5×10^{-4}–1.0×10^{-3}.

(**a**)   (**b**)
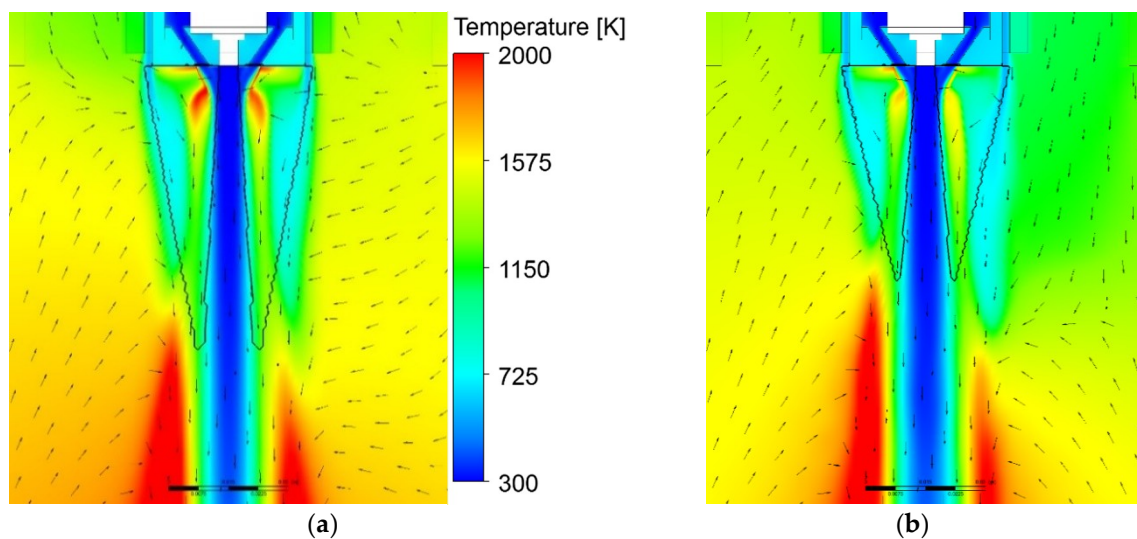
Figure 7. Temperature profiles from CFD simulations for case 1 (**a**) and case 2 (**b**); see Table 3 for details. Arrows correspond to velocity vectors. Black triangles indicate areas used to estimate the jet surroundings temperature.
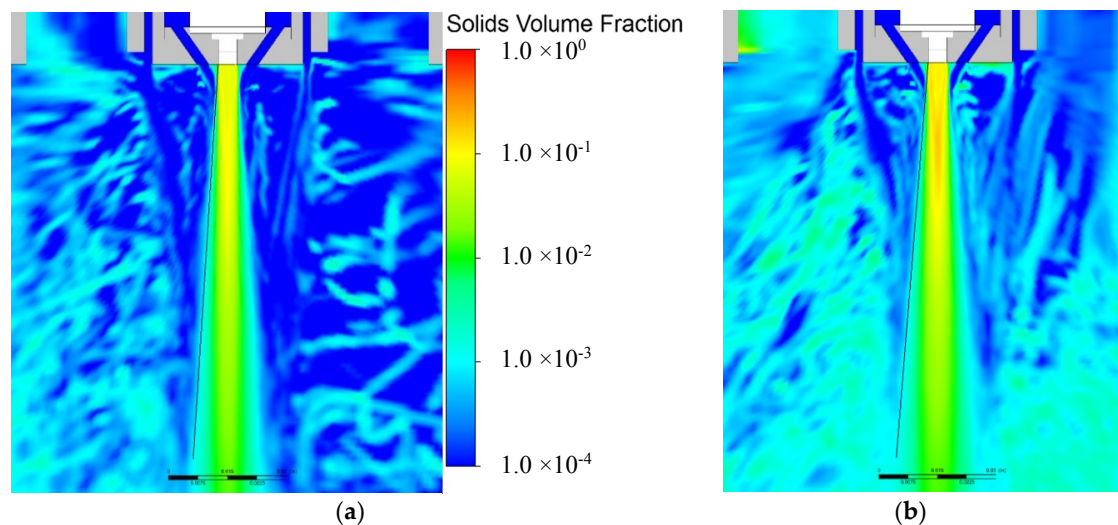
Figure 8. Solids volume fraction profiles from CFD simulations for case 1 (**a**) and case 2 (**b**); see Table 3 for details. Black lines indicate a 0.001 solids volume fraction threshold.

It can be noted that the feed flowrates used in this study are approximately three orders of magnitude less than those of typical commercial entrained flow gasifiers. Nonetheless, commercial gasifiers can have similar, although scaled-up, injector geometries to the one used in this study, resulting in similar gas volumetric fractions in the jet core (i.e., ~0.85). However, the pressure in commercial dry feed gasifiers is typically 2–4 times higher than the pressure applied in this study. This difference in pressure affects the jet core density and the jet surroundings density. Assuming a jet core gas fraction of 0.85 and a solid density of 1200 kg/m^3, increasing the jet gas pressure by a factor of 3 increases the jet core density by a factor of 1.15. Increasing the jet core density by a factor of 1.15 and the jet surroundings density by a factor of 3 in Equation (2) results in an increase of the jet angle by a factor of 1.61. Hence, it is expected that commercial gasifiers will have jet angles ~60% greater than those obtained in this study.

5. Conclusions

Gas-solid jet half-angles were measured using an injector consisting of a central straight tube for solid suspension injection, impinging jets for oxygen injection, and a sleeve for steam injection. The jet half-angles were shown to decrease as the solid/gas loading ratio was increased, which corresponds to an increase of the solid suspension density, and a decrease of the density ratio. This observation is consistent with correlations proposed in previous works. Extension of an existing model, correlating the jet half-angle to the ratio of densities between the jet surroundings and core, was proposed for solid particle jets with solid/gas loading ratios >1. Additionally, the jet half-angle variability was analyzed using a F-test of variances, and it was found that increasing the solid/gas loading ratio (excluding the impinging gas in the calculation), as well as introducing the sleeve gas, had no effect on the jet half-angle variability, while the presence of impinging gas increased the variability. The proposed model was also applied to CFD simulations of the same injector with reactive conditions. The proposed model provided jet half-angle predictions within the range of angles estimated by CFD simulation.

Author Contributions: Conceptualization, all authors; Formal Analysis, F.K. and M.D.; Investigation, F.K. and M.D.; Data Curation, F.K. and M.D.; Writing-Original Draft Preparation, F.K.; Writing-Review and Editing, M.D., A.M., P.M. and R.H.; Visualization, F.K. and M.D.; Funding Acquisition, M.D., R.H., A.M. and P.M.

Conflicts of Interest: The authors declare no conflict of interest.

Nomenclature

Roman Symbols

a	constant for Equation (2) (unitless)
m	mass flow rate (kg/h)
m^*	solid/gas loading ratio (kg_{solid}/kg_{gas})

Greek Letters

ρ	density (kg/m^3)
φ	jet half-angle ($°$)

Subscripts

a	surroundings
g	gas
o	jet core at the injection point
s	solids

References

1. International Energy Agency. *CO₂ Emissions from Fuel Combustion*; Organization for Economic Co-operation and Development: Paris, France, 2012; ISBN 978-92-64-17475-7.
2. Kunze, C.; Spliethoff, H. Assessment of oxy-fuel, pre- and post-combustion-based carbon capture for future IGCC plants. *Appl. Energy* **2012**, *94*, 109–116. [CrossRef]
3. Shi, S.-P.; Zitney, S.E.; Shahnam, M.; Syamlal, M.; Rogers, W.A. Modelling coal gasification with CFD and discrete phase method. *J. Energy Inst.* **2006**, *79*, 217–221. [CrossRef]
4. Fletcher, D.F.; Haynes, B.S.; Christo, F.C.; Joseph, S.D. A CFD based combustion model of an entrained flow biomass gasifier. *Appl. Math. Model.* **2000**, *24*, 165–182. [CrossRef]
5. Sahraei, M.H.; Duchesne, M.A.; Yandon, R.; Majeski, A.; Hughes, R.W.; Ricardez-Sandoval, L.A. Reduced order modeling of a short-residence time gasifier. *Fuel* **2015**, *161*, 222–232. [CrossRef]
6. Sahraei, M.H.; Duchesne, M.A.; Hughes, R.W.; Ricardez-Sandoval, L.A. Dynamic reduced order modeling of an entrained-flow slagging gasifier using a new recirculation ratio correlation. *Fuel* **2017**, *196*, 520–531. [CrossRef]
7. Monaghan, R.F.D.; Ghoniem, A.F. A dynamic reduced order model for simulating entrained flow gasifiers: Part I: Model development and description. *Fuel* **2012**, *91*, 61–80. [CrossRef]
8. Sahraei, M.H.; Yandon, R.; Duchesne, M.A.; Hughes, R.W.; Ricardez-Sandoval, L.A. Parametric Analysis Using a Reactor Network Model for Petroleum Coke Gasification. *Energy Fuels* **2015**, *29*, 7681–7688. [CrossRef]
9. Sahraei, M.H.; Duchesne, M.A.; Hughes, R.W.; Ricardez-Sandoval, L.A. Experimental Assessment, Model Validation, and Uncertainty Quantification of a Pilot-Scale Gasifier. *Ind. Eng. Chem. Res.* **2016**, *55*, 6961–6970. [CrossRef]
10. Monaghan, R.F.D. Dynamic Reduced Order Modeling of Entrained Flow Gasifiers. PhD Thesis, Massachusetts Institute of Technology, Cambridge, MA, USA, 2010.
11. Hedman, P.O.; Smoot, L.D. Particle-gas dispersion effects in confined coaxial jets. *AIChE J.* **1975**, *21*, 372–379. [CrossRef]
12. Modaress, D.; Elghobashi, S.; TAN, H. Two-component LDA measurement in a two-phase turbulent jet. *AIAA J.* **1984**, *22*, 624–630. [CrossRef]
13. Fleckhaus, D.; Hishida, K.; Maeda, M. Effect of laden solid particles on the turbulent flow structure of a round free jet. *Exp. Fluids* **1987**, *5*, 323–333. [CrossRef]
14. Zhang, J.; Zhou, L. Particle behaviors in a pulverized coal-fired sudden-expansion combustor with coaxial jets. *Fuel* **2001**, *80*, 289–299. [CrossRef]

15. Almeida, T.G.; Jaberi, F.A. Large-eddy simulation of a dispersed particle-laden turbulent round jet. *Int. J. Heat Mass Transf.* **2008**, *51*, 683–695. [CrossRef]

16. Sijercic, M.; Belosevic, S.; Stevanovic, Z. Simulation of free turbulent particle-laden jet using Reynolds-stress gas turbulence model. *Appl. Math. Model.* **2007**, *31*, 1001–1014. [CrossRef]

17. Barlow, R.S.; Morrison, C.Q. Two-phase velocity measurements in dense particle-laden jets. *Exp. Fluids* **1990**, *9*, 93–104. [CrossRef]

18. Liu, H.; Cao, W.; Xu, J.; Li, W.; Guo, X.; Sun, Z. Characterization of the granular jet in a coaxial gas stream. *Powder Technol.* **2012**, *225*, 206–213. [CrossRef]

19. Ranz, W.E. Some experiments on orifice sprays. *Can. J. Chem. Eng.* **1958**, *36*, 175–181. [CrossRef]

20. Reitz, R.D.; Bracco, F.V. Ultra-high-speed filming of atomizing jets. *Phys. Fluids* **1979**, *22*, 1054–1064. [CrossRef]

21. Wu, K.-J.; Su, C.-C.; Steinberger, R.L.; Santavicca, D.A.; Bracco, F.V. Measurements of the Spray Angle of Atomizing Jets. *J. Fluids Eng.* **1983**, *105*, 406–413. [CrossRef]

22. Roy, A.; Segal, C.; Joly, C. Spreading Angle and Core Length Analysis of Supercritical Jets. *AIAA J.* **2013**, *51*, 2009–2014. [CrossRef]

23. Beér, J.M.; Chigier, N.A. *Combustion Aerodynamics*; Krieger Publishing Company: Malabar, FL, USA, 1983; ISBN 978-0-89874-545-0.

24. Kus, F.T.; Duchesne, M.A.; Champagne, S.; Hughes, R.W.; Lu, D.Y.; Macchi, A.; Mehrani, P. Pressurized pneumatic conveying of pulverized fuels for entrained flow gasification. *Powder Technol.* **2016**, *287*, 403–411. [CrossRef]

25. Daviault, S.G.; Ramadan, O.B.; Matida, E.A.; Hughes, P.M.; Hughes, R. Atomization performance of petroleum coke and coal water slurries from a twin fluid atomizer. *Fuel* **2012**, *98*, 183–193. [CrossRef]

26. Duchesne, M.A.; Champagne, S.; Hughes, R.W. Dry petroleum coke gasification in a pilot-scale entrained-flow gasifier and inorganic element partitioning model. *Energy Fuels* **2017**, *31*, 6658–6669. [CrossRef]

27. Macchi, A.; Bi, H.; Grace, J.R.; McKnight, C.A.; Hackman, L. Dimensional hydrodynamic similitude in three-phase fluidized beds. *Chem. Eng. Sci.* **2001**, *56*, 6039–6045. [CrossRef]

28. Runstedtler, A.; Yandon, R.; Duchesne, M.; Hughes, R.; Boisvert, P. Conversion of Petroleum Coke in a High-Pressure Entrained-Flow Gasifier: Comparison of Computational Fluid Dynamics Model and Experiment. *Energy Fuels* **2017**, *31*, 5561–5570. [CrossRef]

29. Sauriol, P.; Cui, H.; Chaouki, J. Gas–solid structure in the vicinity of a sparger nozzle in a fluidized bed. *Powder Technol.* **2012**, *228*, 131–140. [CrossRef]